

## Article

# Development of a Polyethylene Breathable Packaging Film with Modified Microcrystalline Cellulose for Fresh Products

Pedro V. Rodrigues , M. Cidália R. Castro \* , Ana M. S. Soares , Liliana Melro  and Ana V. Machado

Department of Polymer Engineering, Institute for Polymers and Composites (IPC), Campus de Azurém, University of Minho, 4804-533 Guimarães, Portugal; pedro.rodrigues@dep.uminho.pt (P.V.R.); nita.soares@hotmail.com (A.M.S.S.); liliana.melro@2c2t.uminho.pt (L.M.); avm@dep.uminho.pt (A.V.M.)

\* Correspondence: cidaliacastro@dep.uminho.pt

**Abstract:** In this study, a material based on polyethylene (PE) and microcrystalline cellulose (MC) was developed as a breathable packaging film. Surface functionalization of MC with 3-aminopropyltriethoxysilane (APTES) has been shown to be an efficient option to tailor their properties and increase opportunities for the application of MC on the reinforcement of polymers such as polyethylene (PE). The functionalization of MC with the mentioned silane derivative was achieved using a green method and later used in the development of composites with PE in three percentages (1, 3, and 5%). All the materials were prepared by melt blending and characterized in terms of structural properties (ATR-FTIR and FTIR in transmittance mode, EDX, and SEM), thermal properties (DSC and TGA), thermomechanical properties (DMA), contact angle measurements and permeability to water vapor. The materials demonstrated the potential to be used as breathable film packaging for fresh products.

**Keywords:** polyethylene composites; microcrystalline cellulose; food packaging; surface functionalization



**Citation:** Rodrigues, P.V.; Castro, M.C.R.; Soares, A.M.S.; Melro, L.; Machado, A.V. Development of a Polyethylene Breathable Packaging Film with Modified Microcrystalline Cellulose for Fresh Products. *Macromol* **2024**, *4*, 269–281. <https://doi.org/10.3390/macromol4020015>

Academic Editor: Giuseppe Cavallaro

Received: 15 March 2024

Revised: 19 April 2024

Accepted: 24 April 2024

Published: 28 April 2024



**Copyright:** © 2024 by the authors. Licensee MDPI, Basel, Switzerland. This article is an open access article distributed under the terms and conditions of the Creative Commons Attribution (CC BY) license (<https://creativecommons.org/licenses/by/4.0/>).

## 1. Introduction

Depending on the type of food, different barrier properties can be required. For example, a packaging film that enables retailers to market fresh foods with extended shelf-life without employing any major processing or chemical additives (like preservatives) would prevent a significant quantity of fresh products from spoiling [1,2].

Recently, due to the interest in environmentally friendly polymer composites, natural fibers have been used, enhancing mechanical properties and biodegradability of the polymer matrix. Cellulose, a natural fiber, is widely used as reinforcement for polymers due to its availability, great mechanical properties, low cost, and biodegradability combined with unique characteristics such as low density, light weight, high specific area (that can interact more strongly with the matrix), and, above all its, makes cellulose a potential eco-friendly additive [3]. Besides these properties, cellulose could also modify the barrier properties of the polymer matrix. However, their hydrophilic character causes poor compatibility with hydrophobic matrices, such as polyethylene [4]. This problem can be easily solved since the presence of repetitive hydroxyl groups on the cellulose surface makes it suitable for several chemical modifications. These changes are essential to increase the compatibility with a polymer matrix, which is an important requirement to achieve good mechanical properties [3,5–7]. Polyethylene (PE) filled with cellulose can have a better compatibility through surface modification of cellulose by the addition of a coupling agent to the matrix. Intensive research on modification strategies of cellulose surface to improve the compatibility degree between cellulose fibers and polymeric matrices has been performed [7–10]. Of all the coupling agents used, silane derivatives seem to be an excellent choice due to the diversity of functional groups and their commercial availability on a large scale. Moreover, the diversity of functional groups in silane coupling materials is a useful strategy that enhances the ability of covalent linkage between cellulose fibers and polymer matrices when two functional groups are presented. Usually, the general structure of silane coupling

agents available is (RO)<sub>3</sub>-Si-R'-X, where alkoxy groups (RO) are capable of reacting with the cellulose surface, rich in OH groups, intermediated by hydrolysis processes, and the other group (R'-X) where R' is an alkyl chain and X is an organofunctional group that can be used to react with the polymer matrix by covalent linkage [11,12]. From all varieties of silane coupling agents, 3-aminopropyltriethoxysilane (APTES), the agent used in this study, is frequently used in silane modification due to its high reactivity, simplistic structure, and low cost resulting in a cellulose-silica composite [13]. Nevertheless, the presence of an amine group on the APTES offers a good compatibilization by covalent linkage, via amine, with PE grafted with maleic anhydride. The modified PE (PE E226) used in this study is FUSABOND<sup>®</sup> E226 resin, which is described by the FDA as a material that can be used for packaging, transporting, or holding food, subject to the limitations and requirements therein.

Therefore, this work aims to develop a methodology to create a breathable material for packaging applications that incorporates modified MC to be chemically bonded to grafted PE, resulting in a continuous matrix with good mechanical and barrier properties. For this, cellulose was first modified with APTES and then the materials were obtained by reactive blending in a mixer. The structure, morphology, and physical properties of the materials were characterized. Studies of surface hydrophobicity were also performed by contact angle measurement and permeability to water vapor and oxygen was carried out to evaluate the barrier properties.

## 2. Materials and Methods

### 2.1. Materials

Polyethylene grafted with maleic anhydride (PE-g-MA, PE E226 FUSABOND<sup>®</sup>) was kindly provided by a Portuguese company. Microcrystalline cellulose (MC) and N,N-dimethylacetamide (DMAc) were supplied from Acros Organics (Waltham, MA, USA), while lithium chloride (LiCl), ethanol, and ammonia solution 25 wt% were purchased from Fisher Chemical (Geel, Belgium). 3-aminopropyltriethoxysilane (APTES) 98% and calcium chloride anhydrous (CaCl<sub>2</sub>) 93% were acquired from Alfa Aesar (Waltham, MA, USA). All materials were used without further purification.

### 2.2. Methods

#### 2.2.1. Microcrystalline Cellulose Modification with 3-Aminopropyltriethoxysilane

The modification of microcrystalline cellulose (MC) surface was carried out using a procedure already reported by Jia et al. [14]. First, a suspension with MC (1.4 g) and LiCl (1.5 g) in N,N-dimethylacetamide (20 mL) was left stirring at 90 °C for 3 h, on a borosilicate glass beaker. Then, 5 mL of the previous MC solution was added to a mixture of ethanol (50 mL)/distilled water (10 mL) and promptly, 2 mL of ammonia solution (25 wt%) and 3-aminopropyltriethoxysilane (1 mL) were added at once to the colloidal solution, which remained under strong stirring at room temperature for 24 h. The white precipitate was separated from the solution through centrifugation, washed with a mixture of water/ethanol, and dried in the oven at 60 °C under vacuum.

#### 2.2.2. Microcomposite Preparation

PE-g-MA and MC-APTES were dried overnight in a vacuum oven at 80 °C to prevent the hydrolysis of polymers during processing. Samples were prepared in a batch mixer (Haake Rheomix Roller Roters R600 (Thermo Scientific<sup>™</sup>, Waltham, MA, USA), volume 69 mL), equipped with two rotors running in a counter-rotating way. Firstly, PE-g-MA was introduced inside the mixer and left around 2.5 min, then MC-APTES was added and a melt temperature of 140 °C, 80 rpm, and 7 min reaction time were used (Table 1). After, all materials were recovered in a metallic plate and left to cool under ambient conditions.

**Table 1.** Composition and processing conditions.

Composition Code	Weight (%)		Processing Conditions		
	PE-g-MA	MA-APTES	T <sub>m</sub> (°C)	Rotors Speed (rpm)	t <sub>mixing</sub> (min)
PE-g-MA_1% MC-APTES	99	1	140	80	2.5 mixing + 7 reaction
PE-g-MA_3% MC-APTES	97	3			
PE-g-MA_5% MC-APTES	95	5			

To achieve our purposes, three materials were prepared adding 1, 3, and 5 wt% of MC-APTES to the melt matrix. From the prepared materials, thin films were produced by compression molding in a hot press at 140 °C under a compressive force of 10 tons on a 5'' diameter ram, with an average thickness of 100 μm.

### 2.3. Characterization

#### 2.3.1. Fourier-Transform Infrared (FTIR) Spectroscopy

The FTIR analysis of the initial and modified materials was conducted on a Jasco 4100 FTIR (Jasco, Easton, MD, USA) spectrometer in ATR and transmittance mode for modified MC-APTES and for the prepared films (PE-g-MA\_MC-APTES), respectively, in the range of 4500–400 cm<sup>-1</sup> using 32 scans and a resolution of 8 cm<sup>-1</sup>.

#### 2.3.2. Thermal Analysis

Thermogravimetric analysis (TGA) was performed using a TA Q500 thermogravimetric analyzer (TA Instruments, New Castle, DE, USA). The samples (approximately 15 mg) were placed in a platinum crucible and heated from 40 °C to 600 °C at a heating rate of 10 °C/min under a nitrogen flow (60 mL/min). The initial decomposition temperature (Tonset), the derivative maximum decomposing rate temperature (Tmax), and the residual weight were determined.

Differential scanning calorimetry (DSC) analysis was accomplished in a Netzsch 200 Maya (Netzsch, Selb, Germany); approximately 4 mg of each sample was cut and placed in an aluminum pan. A heating/cooling ramp was run at 10 °C/min, between 25 °C and 200 °C under nitrogen, for each sample.

The degree of crystallinity  $\chi_c$  was calculated according to Equation (1), as described in [15] as follows:

$$\chi_c(\%) = \frac{\Delta H_m}{W_f \cdot \Delta H_m^0} \times 100\% \quad (1)$$

where  $W_f$  is the PE-g-MA weight fraction,  $\Delta H_m^0$  is the theoretical melting enthalpy of 100% crystalline PE (293 J/g) [16], and  $\Delta H_m$  is the melting enthalpy of our sample.

#### 2.3.3. Scanning Electron Microscopy (SEM)

The morphology of the surface and cross-section of the samples was analyzed using a Leica Cambridge S360 scanning electron microscope (Leica, Berlin, Germany). The samples were previously placed in liquid nitrogen and then fractured, followed by a gold thin coating.

#### 2.3.4. Energy Dispersive X-ray (EDX) Analysis

EDX was performed using a Pegasus X4M (EDAX, Pleasanton, CA, USA) detector coupled to SEM equipment to detect the presence of Si on the sample.

#### 2.3.5. Dynamic Mechanical Analysis (DMA)

Dynamic mechanical analysis measurements were made on rectangular films with the same dimensions (2 cm × 0.5 cm × 100 μm) using a Triton Technology DMA. Samples were evaluated using a dynamic temperature sweep to measure the storage modulus and loss moduli ( $E'$  and  $E''$ ) at a constant frequency (1 Hz), constant force (1 N), and a constant

heating rate of 3 °C/min in oscillatory mode in a range of temperatures between 30 °C and 110 °C. The measurements were made three times for each composite.

### 2.3.6. Contact Angle Measurements (CA)

CA measurements (Contact Angle System OCA 20 Dataphysics, Filderstadt, Germany) were made using distilled water (volume: 3 µL; rate: 2 µL/s) that was dropped on the film surface with a precision syringe using the sessile drop method. The initial image of the drop (taken by 0 s) was recorded with a video camera. At least 20 measurements per film were carried out and the mean value was taken. The contact angles were calculated by the Laplace–Young Fitting method.

### 2.3.7. Water Vapor Permeability (WVP)

The water vapor transmission rate (WVTR) of films was determined by the ASTM method E96 [17]. The desiccant method was used to determine the value of water vapor transmission. The films were placed in circular metal test dishes with a surface diameter of 69.50 mm and filled with ~25 g of anhydrous CaCl<sub>2</sub> previously dried in a vacuum oven at 150 °C overnight. Then, were sealed with parafilm to ensure that humidity migration occurred exclusively through the film. Next, the test cups were placed in a desiccator and kept at room temperature and 94.26 ± 4.33% relative humidity (RH) in triplicate and weighed daily for one month. The measured WVTR of the films was calculated using Equation (2):

$$\text{WVTR} \left( \text{g water} / (\text{m}^2 \times \text{hour}) \right) = \frac{G}{t \times A} \quad (2)$$

where  $G/t$  (g water/h) is the slope (weight versus time plot) and  $A$  is the effective film area (m<sup>2</sup>). WVTR was calculated using three replications and expressed in g·h<sup>-1</sup>·m<sup>-2</sup>.

### 2.3.8. Statistical Analysis

Analysis of variance (ANOVA) and a post hoc Tukey test was used to perform the statistical analysis of the results, using the OriginPro (v. 9.8.0) program.

## 3. Results and Discussion

### 3.1. Structural and Morphological Analysis

The reaction between MC and APTES was performed in solvent; LiCl and DMAc, as a mixture of solvent, is an important factor once the formed complex  $[(\text{DMAc})_2\text{-Li}]\text{Cl}$  penetrates into the cellulose structure, acting as spacers in the MC packing chains, which facilitates the chemical modification [18]. Therefore, the reaction with silane coupling agent, APTES, occurred successfully and could be confirmed by complementary analysis of ATR-FTIR Figure 1 and EDX Figure 3. The modification of MC with APTES was detected by the appearance of an additional peak at 1562 cm<sup>-1</sup>, corresponding to the bending vibration of -NH<sub>2</sub> groups, indicating that they were successfully introduced onto the MC surface. The adsorption peak of Si-O-Si vibration, characteristic of self-condensation, occurred between the silane reaction with cellulose hydroxyl groups at around 1000–1100 cm<sup>-1</sup> and is overlapped with the C-O-C vibration bands of cellulose at around 950–1200 cm<sup>-1</sup>. Moreover, the band corresponding to the Si-O-cellulose, around 1150 cm<sup>-1</sup>, could not be observed due to the presence of the large and intense C-O-C vibration bands of cellulose [13,19,20].

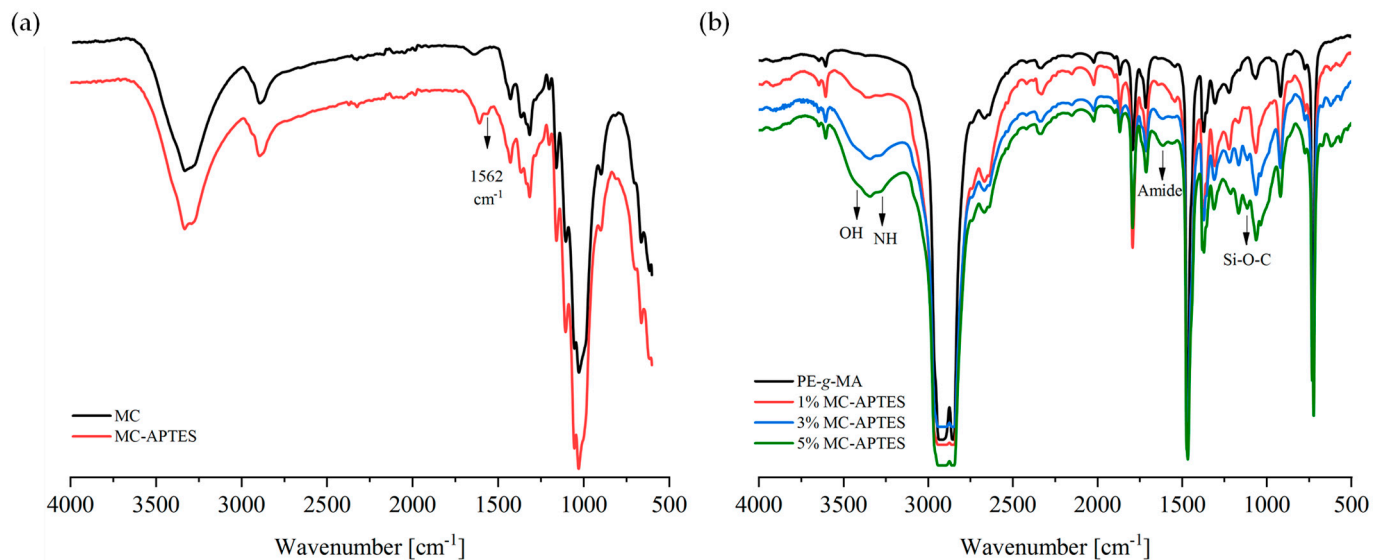
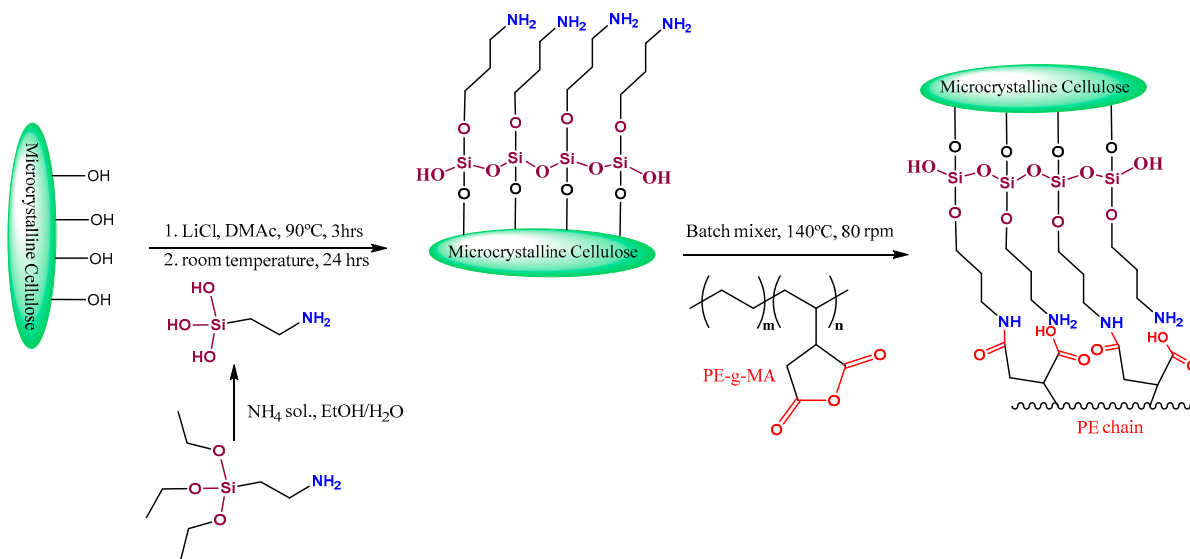


**Figure 1.** (a) ATR-FTIR spectra of MC and MC-APTES and (b) transmittance FTIR spectra of PE-g-MA-MC-APTES films.

After the incorporation of modified cellulose in the polymer, a reaction occurs through amide linkage between the amine group of cellulose-silane and maleic anhydride grafted onto PE, as illustrated on Scheme 1.



**Scheme 1.** Reaction scheme of PE-g-MA and MC-APTES.

According to the ATR-FTIR results (Figure 1a), both samples exhibited absorption peaks that are characteristic of cellulose, namely the peaks at 3318, 2859, 1428, 1315, and 1025  $\text{cm}^{-1}$ , which are associated with the vibration of -OH, C-H, -CH<sub>2</sub>, and C-O, respectively.

Films of the prepared materials and PE-g-MA were analyzed by FTIR in transmittance mode and are depicted in Figure 1b. The covalent linkage between PE-g-MA and modified cellulose was confirmed by the disappearance of the bending vibration -NH<sub>2</sub> at 1562  $\text{cm}^{-1}$ , which demonstrates that the amino groups on the cellulose surfaces were converted to an -NH-band at 3320  $\text{cm}^{-1}$  and an amide band around 1613  $\text{cm}^{-1}$ . Moreover, the band intensity increases with increasing content of modified cellulose and there is also a growth of the broad band related to the -OH groups of cellulose and to the consequent succinic ring opening.

SEM micrographs of PE-g-MA and PE-g-MA containing 5 wt% MC-APTES are represented in Figure 2. Since the micrographs of the materials with 1 and 3 wt% of MC-APTES are very similar to the one with 5 wt% of MC-APTES, only the latter is presented. The surface and cross-section of PE-g-MA film, Figure 2a, revealed smooth and homogeneous surfaces, whereas the film that incorporates MC-APTES exhibits a rough surface, Figure 2b. Moreover, in the cross-section of the same samples, in Figure 2b it is possible to notice that MC-APTES is located along the sample and at the surface. As expected from the chemical results, the modified MC was successfully chemically linked to the polymer matrix.

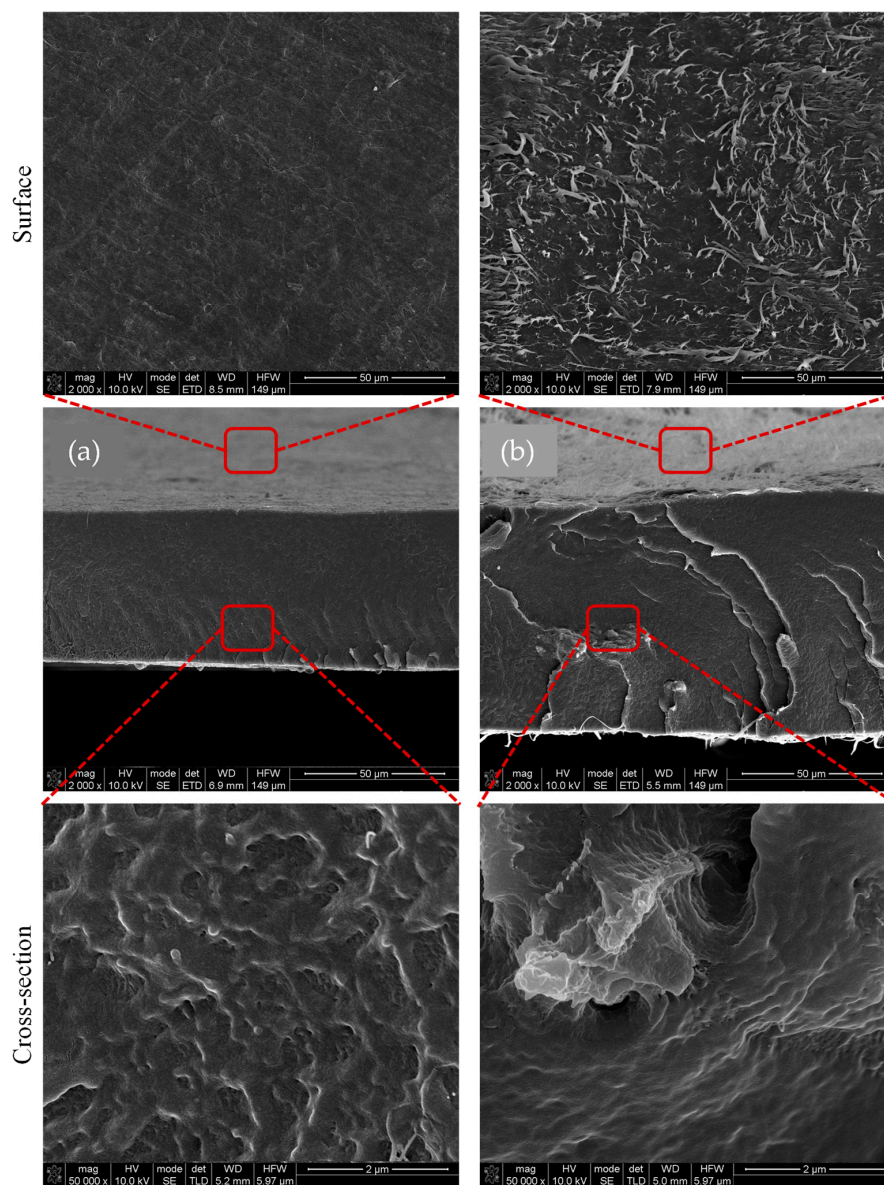


**Figure 2.** Sample surface and cross-section SEM micrographs of (a) PE-g-MA and (b) PE-g-MA + 5%MC-APTES.

The presence of silicon (Si) and oxygen (O) in the polymer matrix assessed by EDX are present in Figure 3. Figure 3a corresponds to the modified MC, where the O and Si peaks have a significant intensity. As expected, a lower intensity can be observed in Figure 3b, which corresponds to the samples containing 5 wt% of MC-APTES, respectively. Even though the peak intensity increased with the amount of MC-APTES incorporated, they are almost undetected for the samples containing 1 wt%. This can be due to the heterogeneous

dispersion of the MC-APTES in the matrix that made the evaluation more complicated since only points are selected in this kind of analysis.

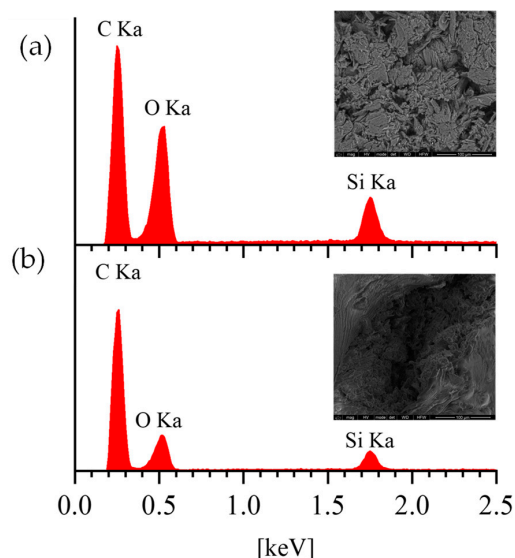


**Figure 3.** EDX spectra of MC-APTES (a) and PE-g-MA reacted with 5% (b) of MC-APTES.

### 3.2. Thermal and Mechanical Analysis

The effect of MC functionalization with APTES on its thermal properties and incorporation in the PE matrix was evaluated (Figures 4 and 5, respectively). Figure 4 depicts the thermal decomposition of MC and modified MC, where it is possible to observe an initial weight loss (~5%) around  $T = 80\text{ }^{\circ}\text{C}$ , for MC, probably due to the vaporization of adsorbed water. The modification of the MC surface with APTES increases both the initial thermal degradation and temperature at the maximum degradation rate, with a difference of around  $10\text{ }^{\circ}\text{C}$  between MC ( $350.6\text{ }^{\circ}\text{C}$ ) and MC-APTES ( $361.2\text{ }^{\circ}\text{C}$ ), as can be seen in Figure 4b. This increase in the thermal stability of MC-APTES may be attributed to the good interaction between the APTES and MC and their consequent crosslinking reactions that occurred during the functionalization. Moreover, the results also demonstrate that for  $T = 500\text{ }^{\circ}\text{C}$  (Figure 4a), MC-APTES have a higher residual mass value than unmodified MC, 26.9 and 14.6%, respectively. This result can be associated with the presence of siloxy moieties on MC-APTES products that remain as a residue. These results are in agreement with the results reported by H. Khanjanzadeh et al. [13].

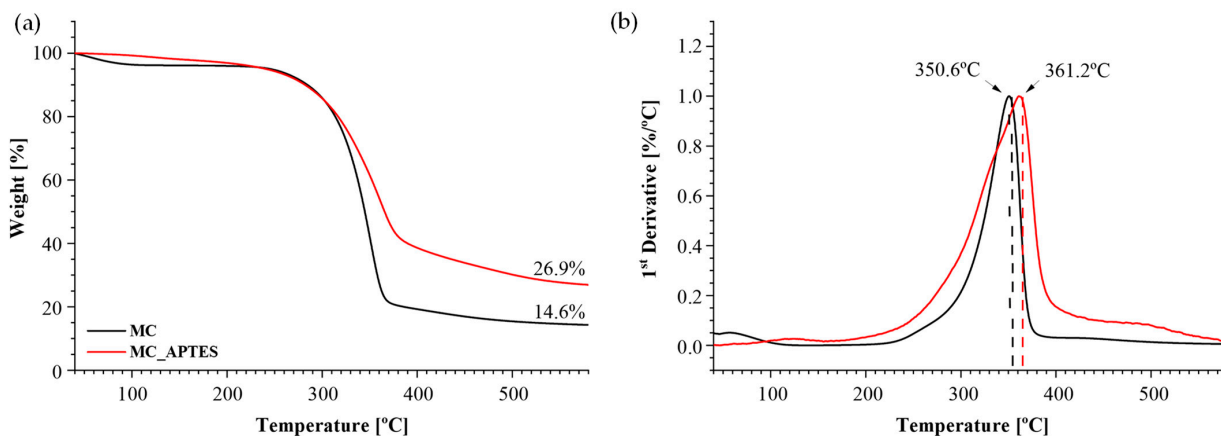


**Figure 4.** TGA curve weight loss (a) and first derivative (b) of unmodified MC and modified MC.

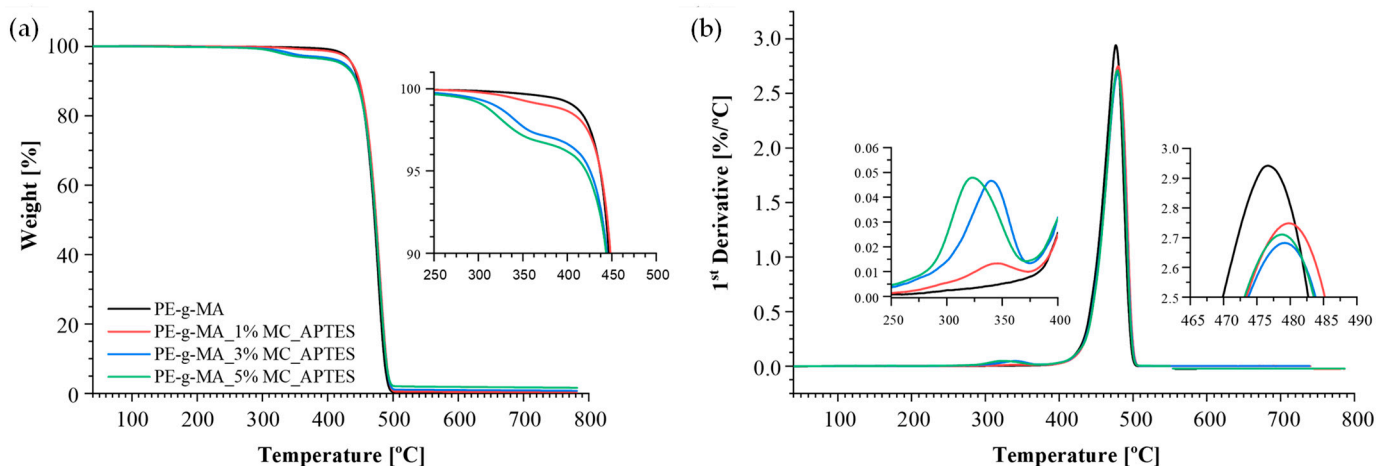


**Figure 5.** TGA curve weight loss (a) and first derivative (b) of PE-g-MA and PE-g-MA-MC-APTES composites.

TGA results of the prepared materials, Figure 5, reveal that despite the fact that an earlier decomposition temperature between 320–343 °C can be noticed, the thermal stability is slightly enhanced since the degradation peak of the PE matrix shifts to higher temperatures. Whereas the curve for PE-g-MA presented only one thermal degradation stage with a mass loss of almost 100%, the curve of the other samples displays two thermal degradation stages. The first degradation peak is related to cellulose degradation (320–343 °C) and, as expected, increasing the MC-APTES amount increases the weight loss (around 4.5%) and a decrease in the decomposition temperature value, Figure 5b. The same occurs for the degradation peak of PE (478–479 °C), the sample with 1%MC-APTES seems to be the most thermally stable composite when compared with the other composites. This is in accordance with the literature; Ch.V.Alexanyan et al. reported a study where it is possible to verify that the presence of cellulosic materials translates into a slight increase in the degradation temperature. Moreover, the charcoal, resulting from cellulose degradation, contributes to the hydrogenation of the unsaturated products and, consequently, the hydrogenated products develop at higher temperatures [21].

The DSC experimental curves of PE-g-MA\_MC-APTES composites obtained from the first heating and cooling cycle are displayed in Figure 6 and Table 2.

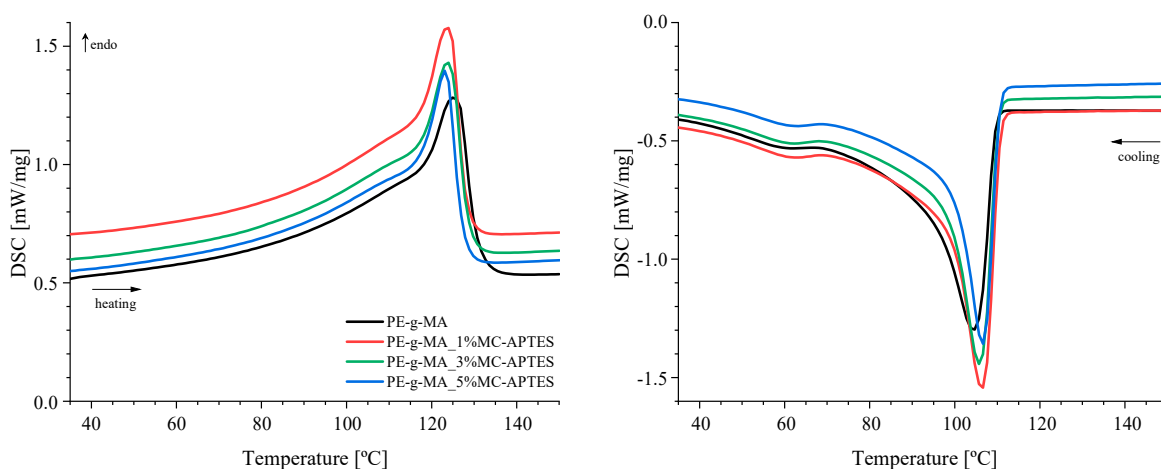


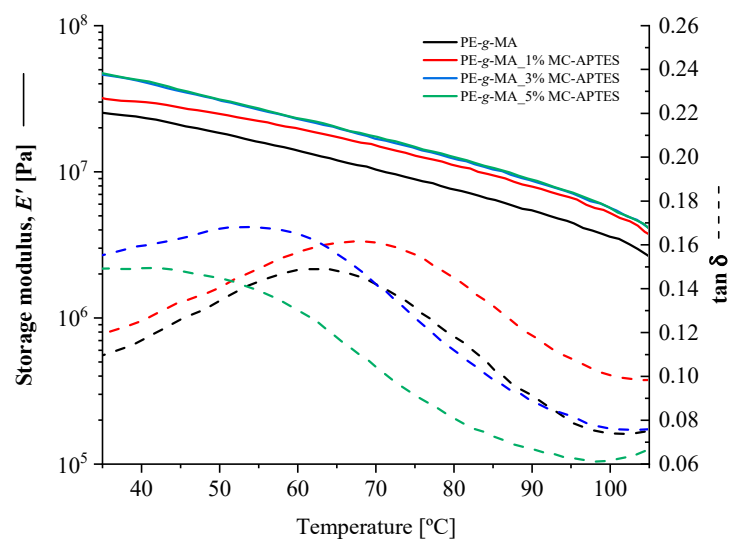
**Figure 6.** Thermal behavior of PE-g-MA and prepared samples.

**Table 2.** DSC results for PE-g-MA composites.

Sample	$\Delta H_m$ [J/g]	$X_c$ [%]	$T_m$ [°C]	$T_c$ [°C]
PE-g-MA	123.9	42.3	125	105
1% MC-APTES	126.8	43.7	124	107
3% MC-APTES	120.3	42.3	124	106
5% MC-APTES	111.8	40.2	123	107

Crystalline polymers are characterized by a melting transition at a certain temperature, the melting temperature ( $T_m$ ), and enthalpy ( $\Delta H$ ) for melting. The crystallinity of the PE was in the range of 40–44% for all studied composites, where the crystallinity of neat PE-g-MA is 42.9%. The presence of MC slightly shifts the melting point of PE-g-MA for lower temperatures, narrowing the peak. This could be evidence that the presence of cellulose in the matrix induces less stable crystals. On the other hand, cellulose can act as a nucleating agent during the cooling cycle, whereas the crystallization peak starts at higher temperatures. Although this results, no significant changes in crystallinity are detected, which cannot be related to the following characterization of the film properties.

Dynamic mechanical results of all materials (Figure 7) exhibited an increase in storage modulus as the amount of modified MC content in the polymer increased. This is associated with the reinforcement effect of the MC. Moreover, the shift of tan delta to lower temperatures is in agreement with  $E'$  enhancement as the shift to lower temperatures indicates a better compatibilization between modified MC and the polymer matrix.

**Figure 7.** Storage modulus (solid) and  $\tan \delta$  (dash) obtained by DMA for neat PE-g-MA and PE\_MC-APTES composites.

### 3.3. Water Affinity Assessment

Polyethylene is known as a hydrophobic polymer, meaning that its wetting ability is very low, which can be a disadvantage in food applications. Therefore, the incorporation of more hydrophilic materials, such as cellulose and/or cellulose-silane composites, could increase the wettability capacity [22].

Distilled water (volume: 3  $\mu$ L; rate: 2  $\mu$ L/s) was dropped on the film surface with a precision syringe using the sessile drop method. The image of the initial drop (taken at 0 s) was recorded with a video camera; the contact angles along with the drop image are depicted in Figure 8. As expected, the increase in MC-APTES content on the PE matrix increases the surface wettability and decreases the contact angle. The CA of PE-g-MA is around 90°, due to the hydrophobic nature of PE, while for the materials with 1, 3, and 5% of MC-APTES, the CA are approximately 83°, 81°, and 79°, respectively. This means

that the surface of the film became more hydrophilic with increasing cellulose content, as already reported in the literature [22–24]. Thus, these results are in agreement with the obtained surface SEM image, Figure 2b, where it is possible to observe the presence of modified cellulose on the film surface. Thus, the effect of cellulose on the hydrophilic character of the prepared materials is visible, since the hydroxyl groups present in cellulose are able to form strong hydrogen bonds with the water molecules. Therefore, it is possible to change the hydrophilicity/hydrophobicity of the material by changing the MC content.

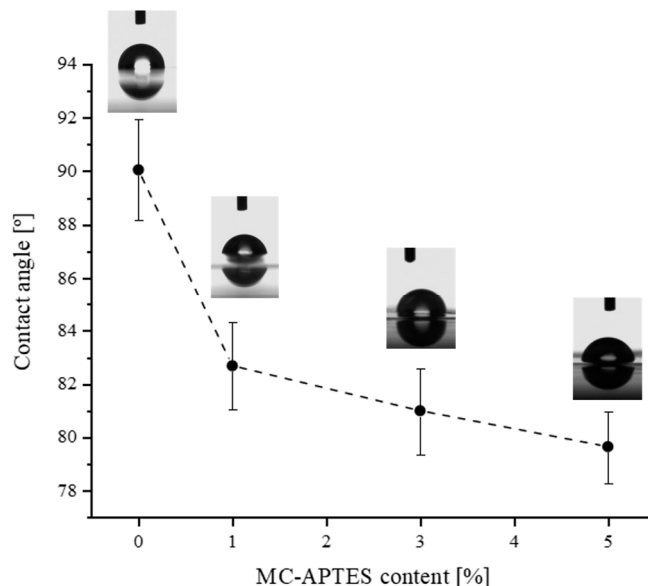


**Figure 8.** Contact angle of PE-g-MA and prepared samples.

The water vapor barrier property is vital for packaging as it can prevent or allow the transmission of this gas from the atmosphere to the food. Therefore, it is crucial to control the transmission of gases/moisture from the environment to the food to extend the shelf life and quality of food [25]. The incorporation of more hydrophilic materials, such as cellulosic derivatives, can change the barrier properties of the gases. Although cellulose displays an effective barrier to gases when it is in a humid environment, cellulose swells; to overcome this drawback and to afford a hydrophobic character, chemical functionalization has been carried out on the cellulose structure [26]. Despite the silanization of the cellulose surface, a smaller number of hydroxyl groups are still available to link water molecules, promoting a path for water vapor.

The WVTR characterizes the capability of moisture to penetrate and pass through the film and it was assessed to understand the effect of MC-APTES content on film water vapor transmission, Figure 9. The results of WVTR demonstrate that the addition of modified cellulose in the PE matrix increased the WVTR of the films from  $0.13 \pm 0.030 \text{ g}\cdot\text{h}^{-1}\text{m}^{-2}$  (PE-g-MA) to  $0.29 \pm 0.026$  and  $0.37 \pm 0.038$  and  $0.69 \pm 0.015 \text{ g}\cdot\text{h}^{-1}\text{m}^{-2}$  of the films with 1, 3, and 5%MC-APTES, respectively. The presence of modified MC results in a lower barrier to water molecules when compared to PE-g-MA and an increase from 3 to 5% MC-APTES raises the WVTR almost twice, namely by  $0.37$  and  $0.69 \text{ g}\cdot\text{h}^{-1}\text{m}^{-2}$ , respectively. This agrees with the literature results, where it is reported that cellulose increases barrier properties due to its solid web-like architecture.

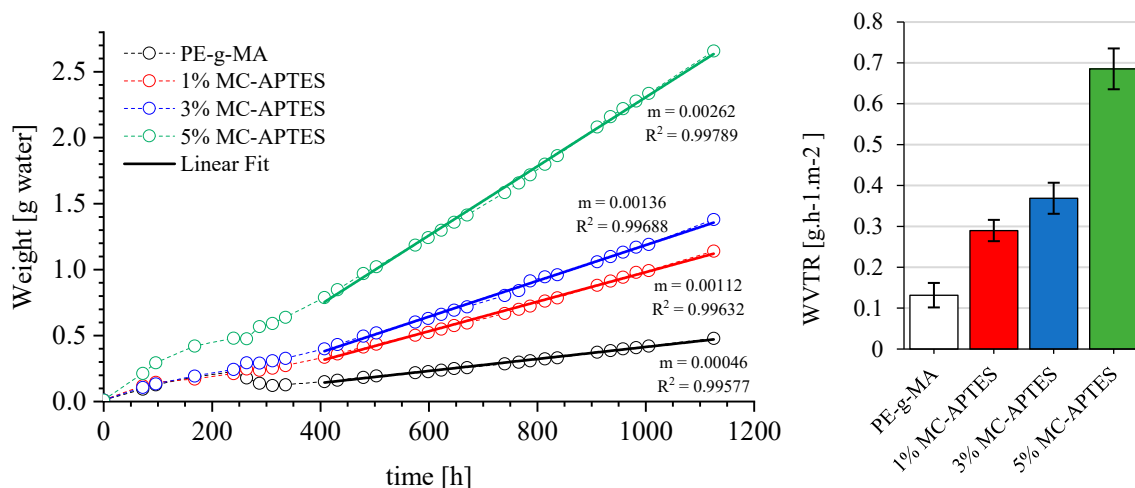


**Figure 9.** Water vapor transmission along time (left) and WVTR (right) of all the material films.

#### 4. Conclusions

An environmentally friendly and simple modification of the MC surface with silane derivatives, as shown in FTIR analysis, and posterior melt blending with PE-g-MA allowed the chemical bonding of both polymer matrix and MC. SEM studies reveal strong interactions between the amino-silane groups attached to the cellulose and the MA grafted in the PE matrix. Consequently, the mechanical properties improved when compared to the polymer matrix. Moreover, the introduction of modified cellulose in the PE matrix results in an increase in thermal stability, shifting the degradation peak of the PE matrix to higher temperatures.

The hydrophilicity and water vapor transmission of produced films can be controlled depending on MC-APTES contents and increasing the MC-APTES content increases the wettability of the film and consequently decreases the CA. For example, the CA of PE-g-MA\_5%MC-APTES composite is significantly lower than for neat PE-g-MA,  $\sim 79^\circ$  and  $\sim 90^\circ$ , respectively, which means more hydrophilic film. Similarly, increasing the MC-APTES content results in higher WVTR compared to neat PE-g-MA.

Therefore, the strategy used allows us to prepare packaging films with good mechanical properties and gas transmission for fresh products.

**Author Contributions:** Conceptualization, M.C.R.C., A.M.S.S. and A.V.M.; methodology, P.V.R., M.C.R.C., A.M.S.S. and A.V.M.; software, P.V.R. and L.M.; validation, A.M.S.S. and A.V.M.; formal analysis, P.V.R., M.C.R.C., A.M.S.S. and A.V.M.; investigation, M.C.R.C., A.M.S.S. and L.M.; resources, A.V.M.; data curation, P.V.R., M.C.R.C., A.M.S.S. and A.V.M.; writing—original draft preparation, A.M.S.S. and L.M.; writing—review and editing, P.V.R., M.C.R.C. and A.V.M.; visualization, A.V.M.; supervision, A.V.M.; project administration, A.V.M.; funding acquisition, A.V.M. All authors have read and agreed to the published version of the manuscript.

**Funding:** This research was funded within the scope of the project TSSiPRO—technologies for sustainable and smart innovative products—NORTE-01-0145-FEDER-000015. The authors also acknowledge the financial support by Portugal 2020 and Fundo Social Europeu (FSE) through Programa Operacional Regional do NORTE (NORTE-08-5369-FSE-000034), developed under the program “IMPULSE—Polímeros e Compósitos: Drivers da inovação tecnológica e da competitividade industrial”.

**Data Availability Statement:** The raw/processed data required to reproduce these findings cannot be shared at this time as the data also form part of an ongoing study.

**Conflicts of Interest:** The authors declare no conflicts of interest.

## References

1. Czerwiński, K.; Rydzkowski, T.; Wróblewska-Krepsztul, J.; Thakur, V.K. Towards Impact of Modified Atmosphere Packaging (MAP) on Shelf-Life of Polymer-Film-Packed Food Products: Challenges and Sustainable Developments. *Coatings* **2021**, *11*, 1504. [[CrossRef](#)]
2. Caleb, O.J.; Mahajan, P.V.; Al-Said, F.A.-J.; Opara, U.L. Modified Atmosphere Packaging Technology of Fresh and Fresh-cut Produce and the Microbial Consequences—A Review. *Food Bioprocess Technol.* **2013**, *6*, 303–329. [[CrossRef](#)] [[PubMed](#)]
3. Miao, C.; Hamad, W. Cellulose reinforced polymer composites and nanocomposites: A critical review. *Cellulose* **2013**, *20*, 2221–2262. [[CrossRef](#)]
4. Yano, H.; Omura, H.; Honma, Y.; Okumura, H.; Sano, H.; Nakatsubo, F. Designing cellulose nanofiber surface for high density polyethylene reinforcement. *Cellulose* **2018**, *25*, 3351–3362. [[CrossRef](#)]
5. Zimniewska, M.; Wladyka-Przybylak, M.; Mankowski, J. Cellulosic Bast Fibers, Their Structure and Properties Suitable for Composite Applications. In *Cellulose Fibers: Bio- and Nano-Polymer Composites—Green Chemistry and Technology*, 1st ed.; Kalia, S., Kaith, B.S., Kaur, I., Eds.; Springer: Berlin/Heidelberg, Germany, 2011; pp. 97–119.
6. Rajak, D.K.; Pagar, D.D.; Menezes, P.L.; Linul, E. Fiber-reinforced polymer composites: Manufacturing, properties, and applications. *Polymers* **2019**, *11*, 1667. [[CrossRef](#)] [[PubMed](#)]
7. Mohit, H.; Arul Mozhi Selvan, V. A comprehensive review on surface modification, structure interface and bonding mechanism of plant cellulose fiber reinforced polymer based composites. *Compos. Interfaces* **2018**, *25*, 629–667. [[CrossRef](#)]
8. Missoum, K.; Belgacem, N.; Bras, J. Nanofibrillated Cellulose Surface Modification: A Review. *Materials* **2013**, *6*, 1745–1766. [[CrossRef](#)] [[PubMed](#)]
9. Abushammala, H.; Mao, J. A Review of the Surface Modification of Cellulose and Nanocellulose Using Aliphatic and Aromatic Mono- and Di-Isocyanates. *Molecules* **2019**, *24*, 2782. [[CrossRef](#)] [[PubMed](#)]
10. Tavakolian, M.; Jafari, S.; van de Ven, T. A Review on Surface-Functionalized Cellulosic Nanostructures as Biocompatible Antibacterial Materials. *Nano-Micro Lett.* **2020**, *12*, 73. [[CrossRef](#)] [[PubMed](#)]
11. Xie, Y.; Hill, C.A.S.; Xiao, Z.; Militz, H.; Mai, C. Silane coupling agents used for natural fiber/polymer composites: A review. *Compos. Part A Appl. Sci. Manuf.* **2010**, *41*, 806–819. [[CrossRef](#)]
12. Jayasuriya, C.K. Interfacial Bonding in Polymer–Ceramic Nanocomposites. In *Reference Module in Materials Science and Materials Engineering*; Elsevier: Amsterdam, The Netherlands, 2017.
13. Khanjanzadeh, H.; Behrooz, R.; Bahramifar, N.; Gindl-Altmatter, W.; Bacher, M.; Edler, M.; Griesser, T. Surface chemical functionalization of cellulose nanocrystals by 3-aminopropyltriethoxysilane. *Int. J. Biol. Macromol.* **2018**, *106*, 1288–1296. [[CrossRef](#)] [[PubMed](#)]
14. Jia, N.; Li, S.-M.; Ma, M.-G.; Zhu, J.; Sun, R.-C. Synthesis and characterization of cellulose-silica composite fiber in ethanol/water mixed solvents. *Bioresources* **2011**, *6*, 1186–1195. [[CrossRef](#)]
15. Tarani, E.; Arvanitidis, I.; Christofilos, D.; Bikiaris, D.N.; Chrissafis, K.; Vourlias, G. Calculation of the degree of crystallinity of HDPE/GNPs nanocomposites by using various experimental techniques: A comparative study. *J. Mater. Sci.* **2023**, *58*, 1621–1639. [[CrossRef](#)]
16. Mirabella, F.; Bafna, A. Determination of the crystallinity of polyethylene/olefin copolymers by thermal analysis: Relationship of the heat of fusion of 100% polyethylene crystal and the density. *J. Polym. Sci. Part B Polym. Phys.* **2002**, *40*, 1637–1643. [[CrossRef](#)]
17. *ASTM E96/E96M-16*; Standard Test Methods for Water Vapor Transmission of Materials. ASTM: West Conshohocken, PA, USA, 2015.
18. Kotov, N.; Raus, V.; Dybal, J. Intermolecular Interactions in N,N-Dimethylacetamide without and with LiCl Studied by Infrared Spectroscopy and Quantum Chemical Model Calculations. *J. Phys. Chem. B* **2018**, *122*, 8921–8930. [[CrossRef](#)] [[PubMed](#)]
19. Liu, Y.; Lv, X.; Bao, J.; Xie, J.; Tang, X.; Che, J.; Ma, Y.; Tong, J. Characterization of Silane Treated and Untreated Natural Cellulosic Fibre from Corn Stalk Waste as Potential Reinforcement in Polymer Composites. *Carbohydr. Polym.* **2019**, *218*, 179–187. [[CrossRef](#)] [[PubMed](#)]
20. Bengtsson, M.; Oksman, K. The use of silane technology in crosslinking polyethylene/wood flour composites. *Composites Part A Appl. Sci. Manuf.* **2006**, *37*, 752–765. [[CrossRef](#)]
21. Lomakin, S.M.; Rogovina, S.Z.; Grachev, A.V.; Prut, E.V.; Alexanyan, C.V. Thermal degradation of biodegradable blends of polyethylene with cellulose and ethylcellulose. *Thermochim. Acta* **2011**, *521*, 66–73. [[CrossRef](#)]
22. Hubbe, M.A.; Ferrer, A.; Tyagi, P.; Yin, Y.; Salas, C.; Pal, L.; Rojas, O.J. Nanocellulose in Thin Films, Coatings, and Plies for Packaging Applications: A Review. *BioResources* **2017**, *12*, 91. [[CrossRef](#)]
23. Dang, X.; Cao, X.; Ke, L.; Ma, Y.; An, J.; Wang, F. Combination of cellulose nanofibers and chain-end-functionalized polyethylene and their applications in nanocomposites. *J. Appl. Polym. Sci.* **2017**, *134*, 45387. [[CrossRef](#)]
24. da S. Junior, O.G.; de Melo, R.P.; do B.C. Sales, R.; Ayres, E.; de O. Patricio, P.S. Processing and characterization of polyethylene/starch/curauá composites: Potential for application as thermal insulated coating. *J. Build. Eng.* **2017**, *11*, 178–186.

- 
25. Siracusa, V. Food Packaging Permeability Behaviour: A Report. *Int. J. Polym. Sci.* **2012**, *2012*, 302029. [[CrossRef](#)]
  26. Fotie, G.; Limbo, S.; Piergiovanni, L. Manufacturing of Food Packaging Based on Nanocellulose: Current Advances and Challenges. *Nanomaterials* **2020**, *10*, 1726. [[CrossRef](#)] [[PubMed](#)]

**Disclaimer/Publisher's Note:** The statements, opinions and data contained in all publications are solely those of the individual author(s) and contributor(s) and not of MDPI and/or the editor(s). MDPI and/or the editor(s) disclaim responsibility for any injury to people or property resulting from any ideas, methods, instructions or products referred to in the content.